Soft Matter

RSC Publishing

PAPER

View Article Online
View Journal | View Issue

Cite this: *Soft Matter*, 2013, **9**, 1066

Viscoelasticity, dielectric anisotropy, and birefringence in the nematic phase of three four-ring bent-core liquid crystals with an L-shaped molecular frame

Nejmettin Avci,[ab] Volodymyr Borshch,[a] Dipika Debnath Sarkar,[c] Rahul Deb,[c] Gude Venkatesh,[c] Taras Turiv,[ad] Sergij V. Shiyanovskii,[a] Nandiraju V. S. Rao*[ac] and Oleg D. Lavrentovich*[a]

Molecular shape is an important factor in determining the material properties of thermotropic liquid crystals (LCs). We synthesized and investigated several LC compounds formed by asymmetrically bent molecules with a rigid four-ring core in the shape of the letter 'L'. We measured the temperature dependencies of dielectric permittivities, birefringence, splay K_1 and bend K_3 elastic constants, splay viscosity η_{splay} and flow viscosities $\eta_{||}$ and $\eta_{\perp}$. The bend–splay anisotropy $\delta K_{31} = K_3 - K_1$ is negative, similar to the case of nematic LCs formed by symmetrically bent molecules of V-shape. The dielectric anisotropy $\Delta\varepsilon$ and birefringence are positive in the entire nematic range. The splay viscosity η_{splay} and the flow viscosities $\eta_{||}$ and $\eta_{\perp}$ are smaller than the viscosities measured for the symmetric V-shaped bent-core materials at similar temperatures. The ratio $\Gamma = \eta_{splay}/\eta_{||,\perp}$ is in the range 5–4 that is typical for rod-like LCs. The reported L-shaped bent-core nematic LCs combine the useful features of bent-core LCs (such as a negative δK_{31}, suitable for formulation of broad-range blue phases) with the relatively low viscosities, a property typical for rod-like LCs and beneficial for electro-optic switching applications.

Received 21st June 2012
Accepted 30th October 2012

DOI: 10.1039/c2sm26448j

www.rsc.org/softmatter

1 Introduction

In a nematic liquid crystal (LC), the anisometric molecules align along a single direction called the director $\hat{\boldsymbol{n}}$.[1,2] The details of molecular shape affect the phase diagrams of LCs and macroscopic properties. The so-called bent-core (BC) materials demonstrate especially intriguing new features as compared to LCs formed by conventional rod-like or disk-like molecules.[3,4] For example, BC LCs have been reported to exhibit a thermodynamically stable biaxial nematic phase,[5,6] giant flexo-electric response,[7] and rather unusual negative values of the bend–splay anisotropy[8–10] defined as the difference between the elastic constants of bend and splay, $\delta K_{31} = K_3 - K_1$. Characterization of their material properties is often not so straightforward as in the case of regular LCs, as the complex molecular shape might facilitate smectic clustering,[11–15] lead to surface anchoring transitions and director variations along the normal to the bounding substrates[16,17] that result in optical features mimicking those of a biaxial order, or facilitate a surface electric polarization contributing to the electro-optic response.[18] Furthermore, the BC LCs have a relatively large rotational viscosity[19–21] which makes it difficult to use them in fast-switching electrooptic devices. It is thus of interest to explore whether the molecular shape might be tuned to preserve the distinctive features of BC mesogens but at the very same time, to reduce the rotational viscosity of the materials.

Typical bent-core molecules are based on a five-ring rigid core in which the central ring represents the bend unit, usually a 1,3 substituted benzene. The angle between two attached arms is 120°. Other forms, such as a five-membered heterocycle, either a 2,5-disubstituted 1,3,4-oxadiazole or a 3,5-disubstituted 1,2,4-oxadiazole that yield a somewhat larger angle of 134°–140°, are also reported.[22] In most cases, the bent-core structure is symmetric, resembling the widely open letter 'V'. For example, in the case of five-ring structures, there are two rings on both sides of the central bent unit. Recently, Sathyanarayana *et al.*[20] characterized a different five-ring structure, with the bend unit connected to three rings on one side and to one ring on the other side. Both arms ended in alkoxy chains. It was found that the material properties are close to those of classic V-shaped BC nematic LCs; in particular, the splay viscosity was slightly larger than the viscosity of BC nematics and significantly higher than the viscosity of nematic LCs based on rod-like molecules. The high splay viscosity was attributed to either the role of molecular weight or the formation of fluctuative clusters.

[a]*Chemical Physics Interdisciplinary Program, Liquid Crystal Institute, Kent State University, Kent, OH, 44242, USA. E-mail: olavrent@kent.edu; Fax: +1 (330) 672-2796; Tel: +1 (330) 672-4844*

[b]*Faculty of Science, Department of Physics, Muğla University, 48000 Kötekli Muğla, Turkey*

[c]*Chemistry Department, Assam University, Silchar-788011, Assam, India. E-mail: drnvsrao@gmail.com; Tel: +91 9435522541*

[d]*Institute of Physics, Kyiv, 03039, Ukraine*

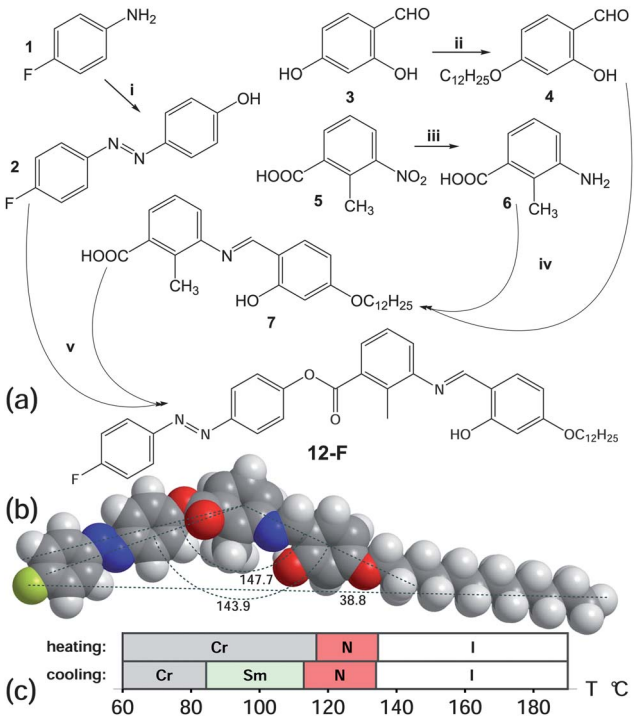

Fig. 1 (a) Synthesis details of the compound **12-F**. *Reagents and conditions*: (i) HCl, $NaNO_2$, 0–5 °C, phenol, NaOH; (ii) dry acetone, $KHCO_3$, $C_{12}H_{25}Br$, KI; (iii)10% Pd/C, H_2, EtOAc, stirring 48 h; (iv) abs. EtOH, AcOH, Δ, 6 h; (v) DCC, DMAP, DCM, stirring 48 h. (b) Energy optimized molecular structure of **12-F** using density functional theory (DFT) studies. (c) The phase transition temperatures for **12-F**.

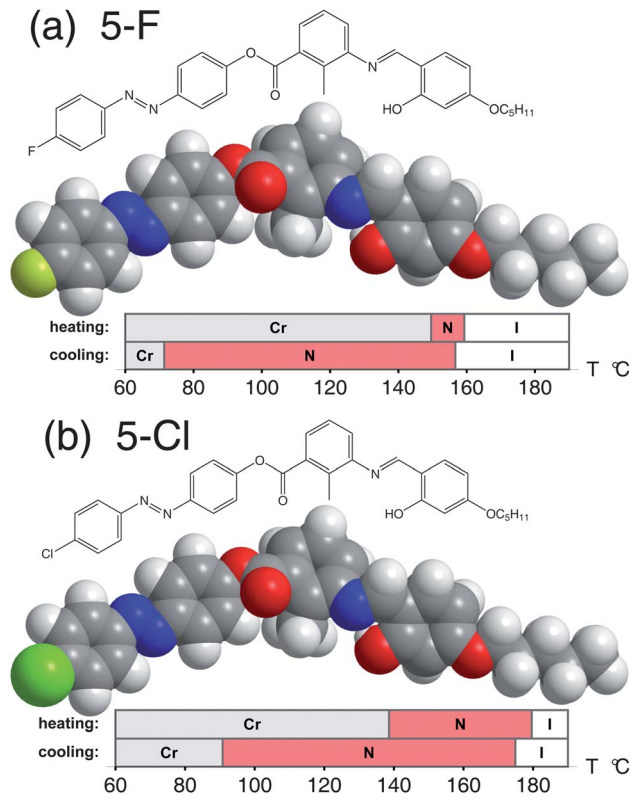

Fig. 2 Molecular structures and phase transition temperatures for the compounds (a) **5-F** and (b) **5-Cl**.

There are currently dozens of five-ring BC molecules synthesized and explored as mesomorphic materials, but only a few reports on BC mesogens with a four-ring frame.[23–31] The first realization was based on asymmetric biphenyls.[23–25] Fergusson and Hird reported a four-ring system that forms chiral smectic A and C phases but no nematic phase.[27] Weissflog *et al.*[29] also reported only smectic phases in four-ring systems and concluded that most of the four-ring compounds are not able to form the so-called "banana" mesophases encountered in the V-shaped five-ring BC compounds. Recently, the banana phases (B1, B7) were reported in the four-ring systems.[30,31] A rare example of a nematic phase in a four-ring system has been presented by Kang *et al.*,[28] but the range of the nematic phase was small, only 4 °C.

In this work, we report on the synthesis and characterization of three LCs, named **12-F**, **5-F**, and **5-Cl**, based on a four-ring bent-core molecular frame, Fig. 1 and 2. In the four-ring core, the central six-membered toluene unit is attached to two different arms. These molecules resemble the letter 'L'. All three compounds show a wide temperature range of a uniaxial nematic phase with promising material properties. First, their bent–splay anisotropy δK_{31} is negative, which can be used in expanding the temperature range of the blue phase mixtures.[32] Second, their viscosities are lower than those reported for classic BC materials with five-ring V-shaped molecules.[10,19,21,33,34]

2 Experimental

2.1 Synthesis

Two materials, **5-F** and **5-Cl**, have been synthesized previously.[35] The higher homologue (4′-fluoro phenyl azo) phenyl-4-yl 3-[*N*-(4′-*n*-dodecyloxy 2-hydroxybenzylidene)amino]-2-methyl benzoate, here after abbreviated as **12-F**, was synthesized following the procedure outlined in Fig. 1(a).

4-Hydroxy 4′-fluoro azobenzene **2.** 4-Hydroxy 4′-fluoro azobenzene was synthesized by the diazocoupling reaction of 4-fluoroaniline with phenol. To 4-fluoroaniline (1.11 g, 10 mmol) were added 10 ml of distilled water containing hydrochloric acid (12 M, 2.5 ml, 30 mmol) and the mixture was heated to dissolve the contents. The solution was then cooled to 0 °C. To the resulting stirred mixture cooled at 0 °C was added, dropwise, a solution of sodium nitrite (0.76 g, 11 mmol) in 10 ml of water. The resulting diazonium chloride was consecutively coupled with an alkaline solution of phenol (0.94 g, 10 mmol) in 10 ml of water containing 0.80 g (20 mmol) of sodium hydroxide with constant stirring. The azo-dye which formed immediately as a yellow precipitate was filtered, washed several times with water and dissolved in diethyl ether and the resulting organic solution dried over anhydrous sodium sulphate.

The crude product obtained after removal of the solvent under reduced pressure was purified by recrystallization from cold hexane, the precipitate was filtered and washed with water and methanol and dried in vacuum. Yield 1.62 g (75%).

IR ν_{max} in cm^{-1}: 1450 ($\nu_{N=N}$, azo); 3374 (ν_{O-H}); ^1H NMR ($CDCl_3$, 400 MHz): $\delta = 5.56$ (s, 1H, –*OH*); 7.83 (d, 2H, $J = 8.4$ Hz, Ar*H*); 7.72 (d, 2H, $J = 8.0$ Hz, Ar*H*); 7.61 (d, 2H, $J = 7.8$ Hz, Ar*H*); 6.76 (d, 2H, $J = 7.8$ Hz, Ar*H*). Elemental analysis calculated for $C_{12}H_9FN_2O$: C, 66.6; H, 4.20%; found. C, 66.5; H, 4.13%.

The intermediate compounds **4** and **6** were prepared following the procedure reported in ref. 35.

[3-(4-*n*-Dodecyloxy-2-hydroxybenzylidene amino)-2-methylbenzoic acid] **7.** An ethanolic solution of 2-methyl-3-aminobenzoic acid (0.5 g, 33 mmol) was added to an ethanolic solution (20 ml) of 4-*n*-dodecyloxy 2-hydroxy benzaldehyde (1.01 g, 33 mmol). The mixture was refluxed with few drops of glacial acetic acid as the catalyst for 4 hours to yield the pale yellow colored Schiff's base. The precipitate was collected by filtration from the hot solution and recrystallized several times from absolute ethanol to produce a pure compound. Yield = 1.2 g (82.7%).

IR ν_{max} in cm^{-1}: 1624 ($\nu_{CH=N}$, imine); 1726 ($\nu_{C=O}$, acid); 3440 (ν_{O-H}, H-bonded); ^1H NMR ($CDCl_3$, 400 MHz): δ = 13.51 (s, 1H, –*OH*); 10.18 (s, 1H, –CO*OH*); 8.33 (s, 1H, –*CH*=N–); 7.88 (d, 1H, J = 8.4 Hz, Ar*H*); 7.33 (*t*, 1H, J = 8.0 Hz, Ar*H*); 7.46 (d, 1H, J = 8.4 Hz, Ar*H*); 2.44 (s, 3H, Ar–CH_3); 7.23 (d, J = 7.8 Hz, 1H, Ar*H*); 6.98 (d, 1H, J = 8.4 Hz, Ar*H*); 6.43 (s, 1H, Ar*H*); 4.04 (*t*, 2H, J = 7.8 Hz, –O–CH_2–); 1.61 (q, 2H, –O–CH_2–CH_2–); 1.29–1.18 (m, 18H, –O–$(CH_2)_2$–$(CH_2)_9$–); 0.90 (*t*, 3H, J = 7.8 Hz, –O–$(CH_2)_{11}$–CH_3). Elemental analysis calculated for $C_{27}H_{37}NO_4$: C, 73.7; H, 8.48%; found. C, 73.5; H, 8.33%.

(4′-Fluoro phenyl azo) phenyl-4-yl 3-[*N*-(4′-*n*-dodecyloxy 2-hydroxybenzylidene)amino]-2-methyl benzoate, **12-F.** The compound 4-hydroxy 4′-fluoroazobenzene **2** (0.22 g, 1 mmol) and 2-methyl 3-[*N*-(4-*n*-dodecyloxysalicylidene)amino]benzoic acid **7** (0.44 g, 1 mmol) and 4-dimethylamino pyridine (DMAP) (2 mg, 0.01 mmol) were dissolved in dry dichloromethane (DCM) (50 ml) under inert atmosphere. A solution of *N*,*N*′-dicyclohexylcarbodiimide (DCC) (0.25 g, 1.2 mmol) in DCM (20 ml) was added to the above mixture and the mixture was stirred at room temperature for 48 h. The white precipitate *N*,*N*′-dicyclohexylurea was removed by filtration and the solvent DCM was evaporated to get the residue from the filtrate. The solid residue was purified by column chromatography on silica gel using hexane/chloroform (9/1) as the eluent followed by recrystallization from absolute ethanol to afford the pure product as a yellowish solid in more than 70% yield. The yellow product was then recrystallized several times from absolute ethanol to get the pure product and dried in vacuum. Yield = 0.46 g (72%).

IR ν_{max} in cm^{-1}: 1624 ($\nu_{CH=N}$, imine); 1747 ($\nu_{C=O}$, ester); 3194 (ν_{O-H}, H-bonded); ^1H NMR ($CDCl_3$, 500 MHz): δ = 13.51 (s, 1H, –*OH*); 8.45 (s, 1H, –*CH*=N–); 8.02–7.99 (m, 5H, ArH); 7.40–7.26 (m, 7H, Ar*H*); 6.52 (d, 2H, J = 6.4, Ar*H*); 4.01 (*t*, 2H, J = 6.8 Hz, –O–CH_2–); 2.68 (s, 3H, Ar–CH_3); 1.82–1.26 (m, 20H, –$(CH_2)_{10}$–); 0.86 (*t*, 3H, –CH_3). Elemental analysis calculated for $C_{39}H_{44}FN_3O_4$: C, 73.4; H, 6.95%; found C, 73.2; H, 6.86%.

The phase diagrams were characterized by differential scanning calorimetry (DSC) and polarizing microscopy (Fig. 3). **12-F** exhibits a uniaxial nematic phase in the heating cycle and uniaxial nematic and smectic A (SmA) phases in the cooling cycle. **5-F** and **5-Cl** demonstrate only a uniaxial nematic phase on both heating and cooling. The phase transition temperatures with enthalpy (kJ mol^{-1}) and entropy (J mol^{-1} K^{-1}) values in parentheses obtained during second heating and cooling cycles at 5 °C min^{-1} are as follows. For **12-F** during heating: *Cr* 116.6 °C (40.5, 103) *N* 134.6 °C (0.231, 0.56) *Iso*, and cooling: *Iso* 134.0 °C (0.245, 0.60) *N* 112.9 °C (0.136, 0.35) *SmA* 84.4 °C (36.3, 101.8) *Cr*. For **5-F** the values for heating: *Cr* 149.6 °C (38.2, 90.5) *N* 159.3 °C (0.224, 0.52) *Iso*, and for cooling: *Iso* 156.7 °C (0.262, 0.61) *N* 71.4 °C (19.1, 55.5) *Cr*. For **5-Cl** the values for heating: *Cr* 138.6 °C (51.2, 124.6) *N* 179.6 °C (0.197, 0.43) *Iso*, and for cooling: *Iso* 174.9 °C (0.205, 0.46) *N* 90.8 °C (18.3, 50.3) *Cr*.

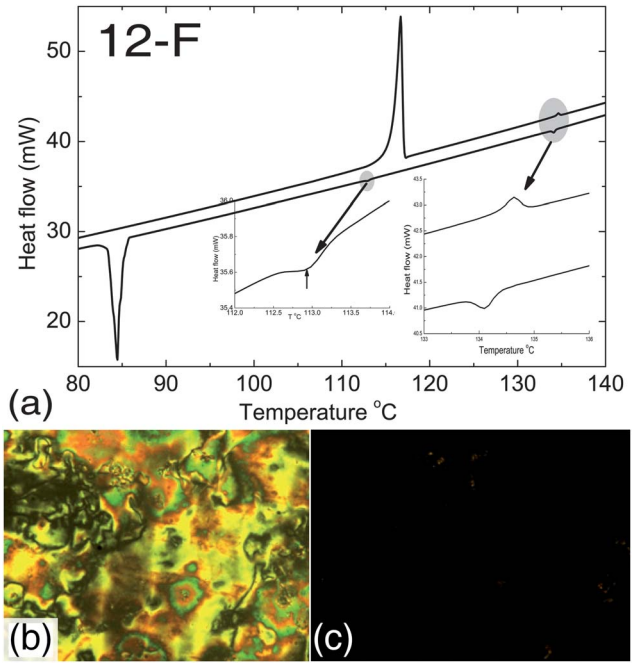

Fig. 3 (a) DSC spectrum of **12-F** obtained in the second heating and cooling cycle at 5 °C min^{-1} with insets showing the Iso–N and N–SmA phase transitions; (b) Schlieren texture of the nematic phase at 130.0 °C; (c) homeotropic texture of the SmA phase at 105.0 °C.

2.2 Material characterization techniques

For dielectric and electrooptical measurements we prepared cells in the following fashion. First, glass plates with a transparent indium tin oxide (ITO) layer were cleaned in an ultrasonic bath filled with a water solution of a detergent. Then the plates were rinsed with deionized water, and cleaned by methanol and ethanol several times, rinsed with isopropanol, and dried at 60 °C. The dried substrates were irradiated with UV light for five minutes in order to remove organic contaminations. Using photolithography, we etched ITO electrodes in a square shape of area 25 mm^2. The substrates were spin-coated with a 1 : 4 solution of the alignment agent PI2555 (HD Microsystems) in T9039 solvent (HD Microsystems), baked at 90 °C for one minute, and then additionally baked at 275 °C for 1 hour. To achieve a uniform planar alignment, the PI2555-coated plates were rubbed with a clean velvet cloth and assembled in an 'antiparallel' fashion. The cells were glued with a UV-curable Norland adhesive NOA-65 containing glass beads as spacers. The cell thickness d was measured by the standard interferometric method. The temperature was controlled by a Linkam hot stage LTS350 and a controller TMS94 with an accuracy of ±0.1 °C.

For dielectric characterization, we used an impedance gain analyser HP4284A that measures complex values of impedance $Z = \mathrm{Re}(Z) + i\mathrm{Im}(Z)$. The effective dielectric permittivity across the planar cell of thickness d was calculated as $\varepsilon = (C_e\omega\mathrm{Im}(Z))^{-1}$, where C_e is the capacitance of the empty cell and ω is the angular frequency of the applied electric field. For these measurements we used a cell of thickness $d = 3.5$ μm for **12-F** and $d = 3.9$ μm for **5-F** and **5-Cl**. A signal generator (Keithley 3390) was used to apply an AC voltage with frequency 25 kHz ($\omega \approx 1.57 \times 10^5$ s^{-1}). We ramped the voltage V from 0.01 V to 2 V in 0.01 V steps and from 2 V to 20 V in 0.1 V increment. The dielectric permittivity for the direction perpendicular to the director, $\varepsilon_\perp$, was determined from the capacitance measured for low voltages, below the Frederiks threshold V_{th} of dielectric reorientation. The parallel component $\varepsilon_{||}$ was measured by extrapolating the voltage dependency of capacitance in the high voltage range, 10–20 V, to $V \to \infty$. The data yield the dielectric anisotropy $\Delta\varepsilon = \varepsilon_{||} - \varepsilon_\perp$.

To determine the elastic constants of splay K_1 and bend K_3, we followed the Saupe technique,[36–38] in which one uses a single planar cell and determines the voltage dependence of its capacitance C. The splay constant is obtained by measuring the Frederiks threshold, $K_1 = \varepsilon_0\Delta\varepsilon V_{th}^2/\pi^2$. For strong surface anchoring, K_3 is extracted by fitting the experimental data well above V_{th} with the expression:[39]

$$\frac{C - C_0}{C_{||} - C_0} = 1 - \frac{2}{\pi}\sqrt{1+\xi}\,\frac{V_{th}}{V}\int_0^1 \sqrt{\frac{1+\kappa x^2}{1+\xi x^2}}\,\mathrm{d}x, \qquad (1)$$

where $\kappa = K_3/K_1 - 1$, $\xi = \varepsilon_{||}/\varepsilon_\perp - 1$, C_0 is the capacitance for $V < V_{th}$, and $C_{||}$ is the capacitance obtained by extrapolating to $1/V = 0$. In order to avoid *trans*- to *cis*-photoisomerization of the azobenzene group, all the dielectric measurements were done in a completely darkened hot stage.[40]

To determine birefringence and splay viscosity, we measured transmission of a polarized light beam through the planar cell of thickness $d \approx 19$ μm, subject to the 25 kHz electric field, Fig. 4. A He–Ne laser (wavelength $\lambda = 633$ nm) was used as a light source. The He–Ne beam promotes *cis*-to-*trans* isomerization of the azobenzene group.[40] The LC cell was placed between two crossed linear polarizers with a rubbing direction at 45° to their extinction directions. The Babinet–Soleil compensator was used to control an additional optical phase retardation. The transmitted light intensity was measured by a photo-detector TIA-525 (Terahertz Technologies Inc.) connected to an oscilloscope Tektronix TDS-2014.

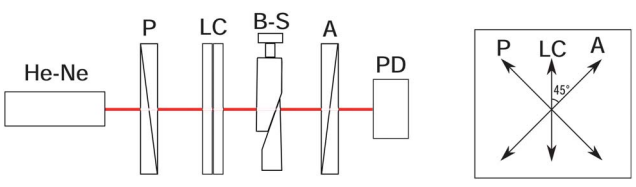

Fig. 4 Electrooptical setup: the LC cell and the Babinet–Soleil compensator (B–S) are placed between a crossed polarizer (P) and an analyser (A). The intensity of the transmitted light of the He–Ne laser is measured by a photodetector (PD).

For the setting shown in Fig. 4, the transmitted light intensity is determined by the voltage-dependent optical phase retardation $\Phi(V)$ of the cell,

$$I(V) = I_0 \sin^2\frac{\Phi(V)}{2}, \qquad (2)$$

where I_0 is the maximum light intensity. By measuring $I(V)$ in the broad range of voltages, from 0 to 20 V, and calculating the interference maxima, we determined the total phase retardation $\Phi_{tot} = 2\pi d\Delta n/\lambda$ of a cell which provides the value of birefringence $\Delta n = n_e - n_o$, where n_e and n_o are the extraordinary and ordinary refractive indices of the LC, respectively.[41]

The splay viscosity is determined by monitoring light intensity changes caused by director relaxation from the state slightly above the Frederiks threshold $V > V_{th}$ to the zero-voltage planar state. As a function of time t elapsed after the voltage is switched off, the light intensity is

$$I(t) = I_0 \sin^2\frac{\Phi_{tot} - \delta(t)}{2}, \qquad (3)$$

where the time-dependent small correction to the total phase retardation shows an exponential decay[42]

$$\delta(t) = \delta_0 e^{-2t/\tau_0}; \qquad (4)$$

from its maximum value δ_0 (at $t = 0$) to 0, with a characteristic decay time τ_0. The slope of dependence $\ln(\delta_0/\delta(t))$ (obtained experimentally with the help of eqn (3)) *versus* time is equal to $2/\tau_0$. The splay viscosity of the LC is then calculated as:[43]

$$\eta_{splay} = \pi^2\tau_0 K_1/d^2. \qquad (5)$$

We also determined effective flow velocities in the direction parallel and perpendicular to the director, by exploring the Brownian motion of colloidal particles in the nematic phase.[22,44,45] We studied poly(methyl methacrylate) (PMMA) spheres of radius $R = 2.7$ μm that align the director tangentially to its surface. The dynamics of isolated particles was monitored using an inverted microscope Nikon Eclipse TE2000-E equipped with a 60× objective and a MotionBlitz EoSens mini1 (Mikrotron GmbH) video camera with a frame rate of 100 fps.[46] The diffusion coefficients for the motion parallel ($D_{||}$) and perpendicular ($D_\perp$) to the director were obtained from the mean square displacement (MSD) of a particle as a function of the lag time τ. A typical time evolution of a particle's MSD at temperature 122 °C is plotted in the inset in Fig. 8. Using the Stokes–Einstein equation, the corresponding viscosities are found as $\eta_{||,\perp} = k_BT/(6\pi RD_{||,\perp})$, where k_B is the Boltzmann constant and T is the absolute temperature.

Separate experiments to explore whether the nematic phase of **12-F**, **5-F**, and **5-Cl** might be of a biaxial type were conducted. For **12-F**, we prepared cells with homeotropic surface anchoring. For homeotropic alignment, we used an inorganic passivation layer NHC AT720-A (Nissan Chemical Industries, Ltd) as well as ITO-coated substrates covered with lecithin. After slow cooling (0.3 °C min^{-1}) from the isotropic phase, the homeotropic alignment was achieved. A polarizing microscope OptiPhot2-Pol (Nikon Instruments, Inc.) with objectives Nikon

MPlan 20×/NA = 0.4 ELWD, MPlan 40×/NA = 0.5 ELWD, and CFPlan 50×/NA = 0.45 SLWD, where ELWD stands for extra-large working distance, SLWD stands for super long working distance, and NA is the numerical aperture, was used for orthoscopic and conoscopic observations.

To discriminate between the uniaxial and biaxial nematic order in the studied materials, we used two approaches. For **12-F**, which can be aligned homeotropically, we used conoscopic studies. **5-F** and **5-Cl** cannot be aligned homeotropically. The test of potential biaxiality in these two materials was based on observation of topological defects formed when small silica spheres (diameter 10 μm, Duke Scientific) were added to the LC[16,47] and when the LC was dispersed as spherical droplets in glycerine.[48]

3 Results and discussion

3.1 Dielectric permittivity

Dielectric permittivity as a function of temperature is shown for all three compounds in Fig. 5(a)–(c). The parallel ($\varepsilon_{||}$) component of dielectric permittivity of **12-F** (Fig. 5(a)) increases with the decrease in temperature and ends up slightly decreasing near the N–SmA phase transition. The perpendicular component ($\varepsilon_{\perp}$) increases as the temperature is lowered. This leads to a non-monotonous behaviour of the dielectric anisotropy ($\Delta\varepsilon = \varepsilon_{||} - \varepsilon_{\perp}$), Fig. 5(d). The average dielectric permittivity $\varepsilon=(\varepsilon_{||} + 2\varepsilon_{\perp})/3$ continues the trend of the isotropic phase permittivity, ε_{iso}, monotonously decreasing with temperature.

The ester group and the fluorine atom on one of the arms of the rigid **12-F** core contribute to the transverse and longitudinal components of the molecular permanent dipole. For **12-F**, the non-monotonous behavior of $\Delta\varepsilon$ with temperature can be explained by the possible formation of smectic cybotactic clusters in the nematic phase.[49,50] In the clusters, molecular separations are much larger in the direction perpendicular to the smectic layers than within the smectic layers. As a result, the longitudinal components of molecular dipoles tend to form antiparallel arrangements within the layers thus reducing $\varepsilon_{||}$. Similarly, the transverse components between the adjacent molecules in the same smectic layer tend to align parallel to each other, increasing $\varepsilon_{\perp}$. The effect explains why $\Delta\varepsilon$ decreases rather dramatically for **12-F** when one approaches the smectic phase by lowering the temperature.

The dielectric permittivity of **5-F** and **5-Cl** shows similar temperature behaviour, Fig. 5(b) and (c). Although these two compounds do not exhibit the smectic phase, $\Delta\varepsilon$ dependence on temperature is also non-monotonous, Fig. 5(d), suggesting that the smectic clusters might form even without the explicit appearance of a homogeneous smectic state. This result is in agreement with the recent demonstration by transmission electron microscopy of smectic clusters in a broad temperature range (tens of degrees) of a uniaxial nematic phase for a BC compound that does not have a stable smectic phase.[51]

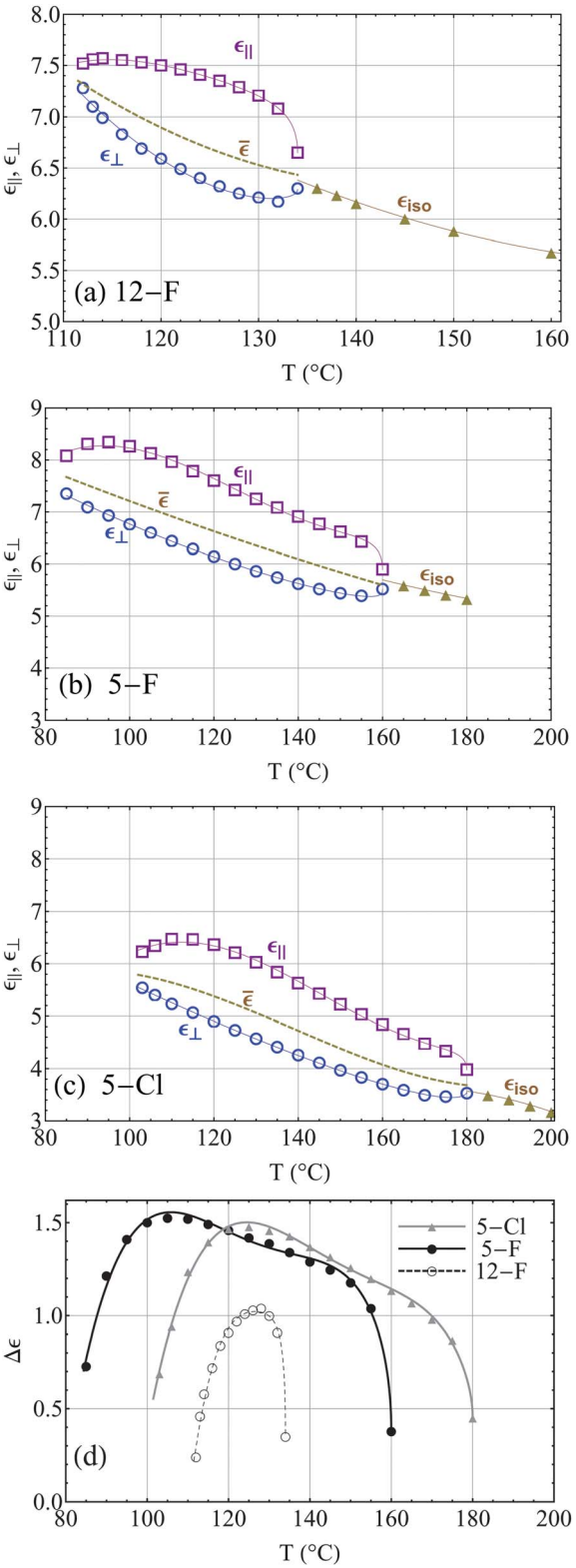

Fig. 5 Temperature dependence of dielectric permittivities for (a) **12-F**, (b) **5-F**, and (c) **5-Cl**. Figure (d) shows the temperature dependence of the dielectric anisotropy. The lines are guides to the eye.

3.2 Splay and bend elastic constants

The bend–splay anisotropy $\delta K_{31} = K_3 - K_1$ in rod-like LCs is typically positive when the nematic is formed by prolate molecules and negative for oblate molecules.[52–55] Recently, it was shown that in BC LCs, $\delta K_{31} < 0$,[8,9,20,33,56] which is a natural result because of the bent shape of BC molecules. Our data

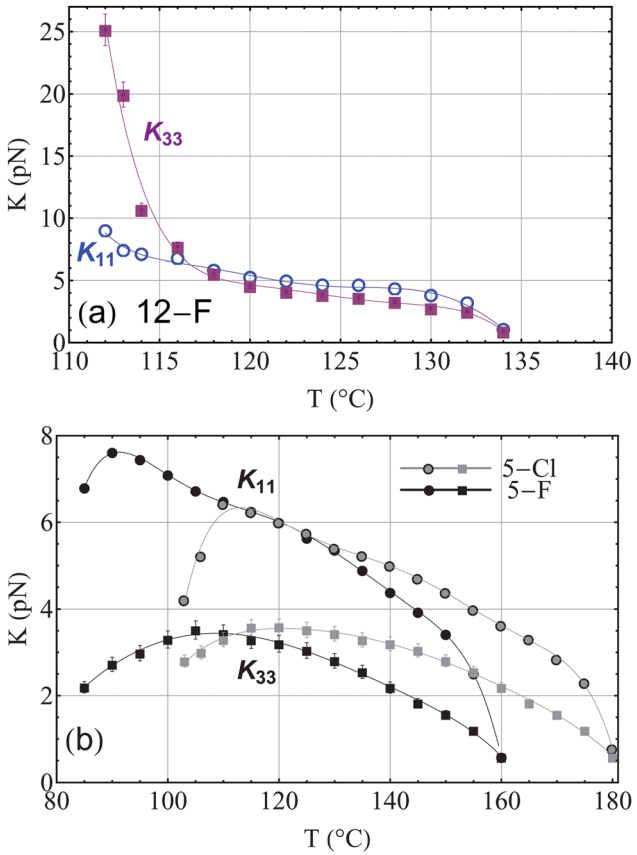

Fig. 6 Splay (circles) and bend (squares) elastic constants *vs.* temperature for (a) **12-F**, (b) **5-F** and **5-Cl**.

demonstrate that in all three L-shape BC LCs, δK_{31} is also negative in a relatively broad temperature range, Fig. 6(a),(b). In **12-F** δK_{31} becomes positive as the temperature is reduced towards the smectic phase, Fig. 6(a). The latter is explained by a strong pre-transitional divergence of K_3 as bend deformations are incompatible with the equidistance of smectic layers.[1,2] The compounds **5-F** and **5-Cl** do not exhibit the smectic phase, and the behaviour of K_3 is similar to that reported by Kaur *et al.*[57]

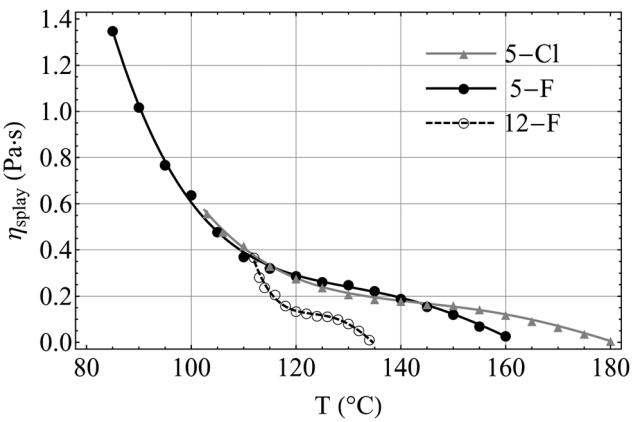

Fig. 7 Temperature variation of the splay viscosity η_{splay} for **12-F** (open circles), **5-F** (closed black circles), and **5-Cl** (grey triangles).

3.3 Splay viscosity and flow viscosities

The splay viscosity η_{splay} for all three compounds, determined from the director relaxation in the Frederiks splay transition, shows a monotonous increase as the temperature is lowered, with a tendency to diverge near the transition to a higher ordered phase, Fig. 7. Its value is noticeably smaller as compared to other BC LCs with a similar nematic temperature range. For example, we find that at $T = 120$ °C, $\eta_{splay} = 0.14$ Pa s for **12-F** and $\eta_{splay} \sim 0.3$ Pa s for both **5-F** and **5-Cl**. For a five-ring hockey-stick nematic LC, the viscosity is noticeably higher:[20] $\eta_{splay} \sim 0.6$ Pa s at the same temperature $T = 120$ °C. For the symmetric V-shaped compound, the reported[34] viscosity is $\eta_{splay} = 0.2$ Pa s at $T = 147.5$ °C, which is much larger than η_{splay} measured for **12-F** at temperatures above 120 °C (Fig. 7).

The splay viscosity of all three studied L-shaped compounds remains higher than that of the rod-like nematics at similar temperatures ($\eta_{splay} = 5.9$ mPa s for PAA at 125 °C (ref. 43) and $\eta_{splay} = 20$ mPa s for M957 at 114 °C (ref. 58)) but is comparable to η_{splay} of rod-like nematics measured at room temperature.[42,58,59]

The splay viscosity is expressed through the rotational viscosity γ_1 and Leslie coefficients α_i as $\eta_{splay} = \gamma_1 - \alpha_3^2/\eta_b = \alpha_3 - \alpha_2 - 2\alpha_3^2/(\alpha_4 + \alpha_5 - \alpha_2)$, where η_b is the viscosity in Miesowicz geometry with the flow parallel to the fixed orientation of the director[60] (η_b is close to the value $\eta_{||}$ determined from the Brownian motion experiment, see below). For the rod-like LCs, α_3 is typically very small, and thus $\eta_{splay} \cong \gamma_1$. For the BC materials, α_3 has not been reported so far, thus we keep the notation η_{splay} in our discussion. We conclude that η_{splay} in **12-F**, **5-F**, and **5-Cl** is intermediate between the values typically found in BC and rod-like LCs at comparable temperatures.

The flow viscosities $\eta_{||}$ and $\eta_\perp$ for **12-F** are shown in Fig. 8. Since the data were obtained for relatively weak tangential surface anchoring, the two quantities can be considered as approximately equal to the Miesowicz viscosities[45] measured for the flow parallel (η_b) and perpendicular (η_a) to the fixed director, namely, $\eta_{||} \cong \eta_b = (\alpha_3 + \alpha_4 + \alpha_6)/2$ and $\eta_\perp \cong \eta_a = \alpha_4/2$. As expected, $\eta_{||} < \eta_\perp$ at all temperatures. The values of $\eta_{||}$ and $\eta_\perp$

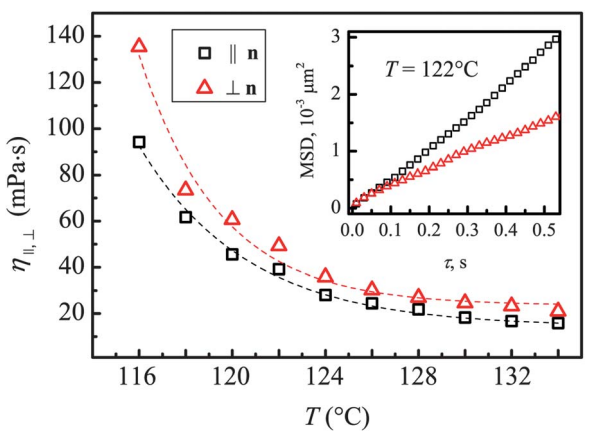

Fig. 8 Flow viscosities $\eta_{||}$ and $\eta_\perp$ for **12-F** as a function of temperature. The inset shows a typical mean-square displacement (MSD) of the probe particle *vs.* time at 122 °C.

in **12-F** for the temperature range 113–135 °C are very close to those of 5CB in the range 23–35 °C.[61] As compared to the rod-like LCs with a nematic temperature range similar to that of **12-F**, the flow viscosities in **12-F** are higher. For example, the literature data list η_a and η_b as 3.4 mPa s and 2.4 mPa s at 122 °C for PAA;[60] 14 mPa s and 9 mPa s at 133 °C for ethyl *p*-[(*p*-methoxybenzylidene)amino] cinnamate,[62] respectively.

The data above allow us to estimate the splay-to-flow viscosity ratios $\Gamma_{||} = \eta_{splay}/\eta_{||}$ and $\Gamma_{\perp} = \eta_{splay}/\eta_{\perp}$ for **12-F**. For $T = 122$ °C, we find $\Gamma_{||} = 5$ and $\Gamma_{\perp} = 4$. These values are comparable to those for rod-like LCs, such as 5CB at 25 °C ($\Gamma_{||} = 3.5$ and $\Gamma_{\perp} = 2.1$)[43] and PAA at 125 °C ($\Gamma_{||} = 3$ and $\Gamma_{\perp} = 2$).[43] Our results are also not very different from the results of Sathyanarayana[21] ($\Gamma_{||} = 16$ and $\Gamma_{\perp} = 12$) for a 43% mixture of V-shaped BC with 5CB at $T \approx 40$ °C. On the other hand, our data differ significantly from $\Gamma = (0.01 - 0.02)$ determined for a V-shaped BC at $T = 70$ °C by Dorjgotov *et al.*[19] Such a drastic difference in Γ's is caused mainly by the difference in the flow viscosities $\eta_{||}$ and $\eta_{\perp}$, as these in **12-F** appear to be at least 10^3 times smaller than those measured[19] for V-shaped BC nematics. One of the possible reasons might be the difference in molecular shapes (the BC molecules studied in ref. 19 have a five-ring rigid core and two aliphatic chains). The other possible reason might be related to the difference in experimental techniques used to determine flow velocities. In ref. 19, the flow velocity was measured by the Quincke rotation technique in which a cylindrical particle rotates in a nematic host, while in our case, the tracked motion is a random Brownian diffusion.

3.4. Birefringence

Birefringence Δn of **12-F** in the nematic phase is relatively high, reaching a maximum value of 0.175 near the transition to the smectic phase, Fig. 9. For **5-F** and **5-Cl**, the birefringence is higher. Their temperature dependencies are standard, with Δn monotonously increasing when the temperature is lowered.

3.5 Biaxiality tests

In the uniaxial nematic phase, the director $\hat{\boldsymbol{n}}$ is also the local optic axis of the material. In the hypothetical biaxial nematic phase, there are three directors usually labelled $\hat{\boldsymbol{n}}$, $\hat{\boldsymbol{m}}$, and $\hat{\boldsymbol{l}}$, that correspond to the orientational order of all three principal axes of the molecules. In the biaxial nematic, there are two optic axes with an angle between them that is determined by the values of three refractive indices. The simplest test of potential biaxiality consists in preparing a homeotropic cell in which the director $\hat{\boldsymbol{n}}$ is perpendicular to the flat bounding plates. If the material is uniaxial, the single optic axis is also perpendicular to the bounding plates. If the material is biaxial, the two optic axes should be tilted away from the direction of $\hat{\boldsymbol{n}}$. The difference is easy to establish by observing the sample in the conoscopic mode (for more details, see ref. 16 and 17).

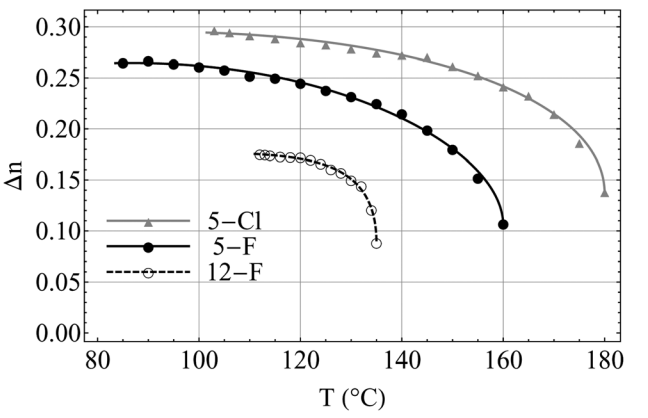

Fig. 9 Temperature dependence of birefringence Δn in the nematic phase of **12-F**, **5-F**, and **5-Cl**.

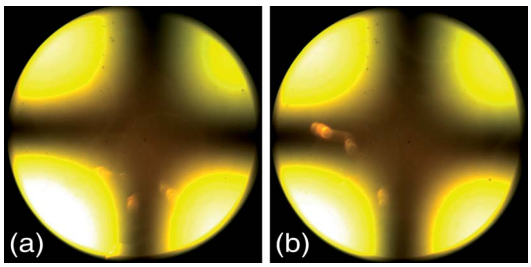

Fig. 10 Conoscopic Maltese cross texture of a homeotropic **12-F** cell of thickness $d = 19$ μm observed with 20× objective between crossed polarizers, at temperature 130 °C. The images (a) and (b) were taken for two orientations of the cell that differ by 45°.

Fig. 10 shows the conoscopic texture of the homeotropically aligned **12-F** cell viewed between crossed polarizers. The texture has the shape of a symmetric 'Maltese cross' with four dark brushes, the so-called isogyres. The texture remains unchanged when the sample is rotated in the plane of view, demonstrating that there is no in-plane ordering in the homeotropic sample and that the optic axis of the sample remains parallel to the direction of observation. The Maltese cross texture persists in the entire temperature range of the nematic phase of **12-F**, demonstrating that the nematic phase is of a uniaxial type. The rate of temperature change was slow, 0.3 °C min^{-1}, to avoid director tilt and apparent optical biaxiality associated with thermal expansion.[63]

Since the materials **5-F** and **5-Cl** cannot be aligned homeotropically in the flat cells, we used different approaches to test their potential biaxiality, based on the features of topological defects in confined geometries.[16,17]

The first experiment is to disperse colloidal silica spheres in the LC cell of thickness $d \approx 50$ μm with a uniform director

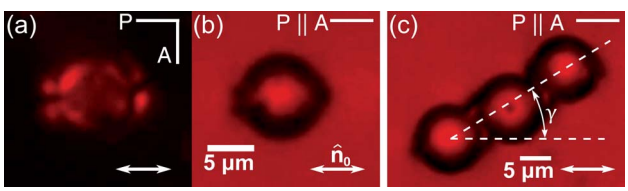

Fig. 11 Colloidal silica spheres in a planar **5-Cl** cell at 165 °C. An isolated sphere with two boojums at poles viewed (a) between two crossed polarizers; (b) between two parallel polarizers. (c) An aggregated chain of spheres, tilted by ≈30° with respect to the overall director $\hat{\boldsymbol{n}}_0$ set by rubbing.

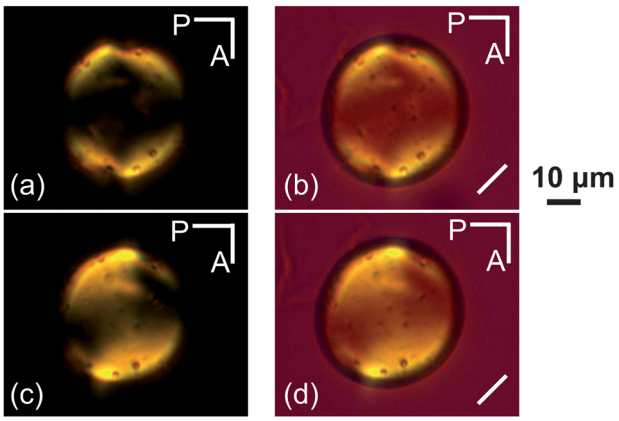

Fig. 12 Polarizing microscopy textures of a **5-F** nematic droplet dispersed in glycerine, viewed between two crossed polarizers (a and c) and with an additional wavelength compensator; the slow axis orientation of the compensator is indicated in the bottom right corner of parts (b and d). Images (c and d) were taken after the sample was rotated by about 15°.

$\hat{\boldsymbol{n}} = \hat{\boldsymbol{n}}_0$ set by rubbing the bounding plates and to observe the director distortions around the particles. Polarizing microscopy shows that the director aligns parallel to the surface of spheres, Fig. 11(a). The director field defined at the spherical surface must contain a certain number of point singularities with the total topological charge equal to 2, according to the Poincaré theorem. In a uniformly aligned uniaxial nematic, the most energetically stable is a configuration with two point defects–boojums located at the axis that is parallel to the overall director $\hat{\boldsymbol{n}}_0$, each of them of a topological charge equal to 1 (as the director rotates by an angle 2π when one circumnavigates the defect core once). The structure expected for the uniaxial nematic is compatible with the experimental texture, in which each sphere is accompanied by two point defects; the imaginary line that connects the point defects is parallel to the overall director $\hat{\boldsymbol{n}}_0$. These textures do not change in the entire range of the nematic phase of both **5-F** and **5-Cl**.

Can the textures in Fig. 11 be made compatible with the biaxial nematic order in the surrounding LC? The answer is negative. The reason is that the defects of topological charge 1 at a surface of a biaxial nematic cannot be isolated point defects. They must represent the ends of singular lines (disclinations) of strength 1 terminating at the surface.[64] These lines are not observable in the textures of **5-F** and **5-Cl**. One might argue that their contrast is too low to allow for direct observation under the microscope. The disclinations should reveal themselves in particle assemblies. In the biaxial nematic, the disclinations are expected to run along the overall director $\hat{\boldsymbol{n}}_0$ and should guide the chaining of the spheres along the same direction $\hat{\boldsymbol{n}}_0$.[16,17] However, this is not what is observed in **5-F** and **5-Cl**: the assembled spheres form chains that are tilted by about 30° with respect to $\hat{\boldsymbol{n}}_0$, Fig. 11(c). The latter configuration is compatible with the behaviour of the tangentially anchored spherical colloids in a uniaxial nematic phase[47] but not with the expected self-assembly of spheres in a biaxial nematic.

In the second experiment, we prepared spherical droplets of **5-F** in glycerine. The droplets show characteristic bipolar textures with two surface point defects–boojums at the poles[48] that do not change with temperature in the entire range of the nematic phase, Fig. 12.

If it were the biaxial nematic phase, the two points should be either connected by a linear defect or merge into a single surface point defect of charge 2. In the biaxial nematic, the smallest charge of the isolated surface point defect is 2.[65]

The above experiments demonstrate that all the studied materials **12-F**, **5-F**, and **5-Cl** show only a uniaxial orientation order (as opposed to the biaxial one) in the entire range of the nematic phase.

4 Conclusions

We explored the properties of the uniaxial nematic phase of three bent-core nematic LCs: **12-F**, **5-F**, and **5-Cl**, with four-ring rigid molecular frames bent in the shape of the letter 'L'. The materials show properties intermediate between those of LCs formed by rod-like and V-shaped five-ring bent-core molecules. All compounds demonstrate a relatively wide temperature range of the uniaxial nematic phase. The elastic bend–splay anisotropy, $\delta K_{31} = K_3 - K_1$, is negative, which might be of interest in formulating wide temperature range blue phase mixtures.[66] The relatively low viscosities η_{splay}, $\eta_{||}$, and $\eta_{\perp}$ as compared to other BC LCs might be of interest for electro-optical applications with a short response time. We found that the ratio $\Gamma_{||,\perp} = \eta_{\text{splay}}/\eta_{||,\perp}$ is on the order of a few units, close to the values reported on the majority of other types of nematic materials. The studied three compounds do not display a biaxial nematic phase. The experimental results add to a general understanding of structure–property relationships in LCs formed by molecules of complex shapes, showing that the L-shaped molecules, being structurally intermediate between the rod-like and V-shaped BC mesogens, yield similarly intermediate macroscopic characteristics of the uniaxial nematic phase.

Acknowledgements

This work was supported by DOE grant #DE-FG02-06ER 46331 (dielectric, splay viscosity, and elastic measurements), NSF DMR 1104850 (flow viscosities) and by Samsung Electronics Corp. N.A. acknowledges support from The Council of Higher Education of Turkey. D.D.S., G.V. and N.V.S.R. acknowledge financial support from Directorate of Naval Research and Development (DNRD) and Department of Science and Technology (India).

Notes and references

1 P. G. de Gennes and J. Prost, *The Physics of Liquid Crystals*, Clarendon Press; Oxford University Press, Oxford, New York, 2nd edn, 1993.
2 M. Kleman and O. D. Lavrentovich, *Soft Matter Physics: An Introduction*, Springer, New York, London, 2003.
3 H. Takezoe and Y. Takanishi, *Jpn. J. Appl. Phys., Part 1*, 2006, **45**, 597–625.

4 R. A. Reddy and C. Tschierske, *J. Mater. Chem.*, 2006, **16**, 907–961.
5 B. R. Acharya, A. Primak and S. Kumar, *Phys. Rev. Lett.*, 2004, **92**, 145506.
6 L. A. Madsen, T. J. Dingemans, M. Nakata and E. T. Samulski, *Phys. Rev. Lett.*, 2004, **92**, 145505.
7 J. Harden, B. Mbanga, N. Eber, K. Fodor-Csorba, S. Sprunt, J. T. Gleeson and A. Jákli, *Phys. Rev. Lett.*, 2006, **97**, 157802.
8 B. Kundu, R. Pratibha and N. V. Madhusudana, *Phys. Rev. Lett.*, 2007, **99**, 247802.
9 P. Sathyanarayana, M. Mathew, Q. Li, V. S. S. Sastry, B. Kundu, K. V. Le, H. Takezoe and S. Dhara, *Phys. Rev. E*, 2010, **81**, 010702.
10 M. Majumdar, P. Salamon, A. Jákli, J. T. Gleeson and S. Sprunt, *Phys. Rev. E*, 2011, **83**, 031701.
11 C. Tschierske and D. J. Photinos, *J. Mater. Chem.*, 2010, **20**, 4263–4294.
12 R. Y. Dong, *Int. J. Mod. Phys. B*, 2010, **24**, 4641–4682.
13 C. Keith, A. Lehmann, U. Baumeister, M. Prehm and C. Tschierske, *Soft Matter*, 2010, **6**, 1704–1721.
14 O. Francescangeli and E. T. Samulski, *Soft Matter*, 2010, **6**, 2413–2420.
15 V. Domenici, *Soft Matter*, 2011, **7**, 1589–1598.
16 B. Senyuk, H. Wonderly, M. Mathews, Q. Li, S. V. Shiyanovskii and O. D. Lavrentovich, *Phys. Rev. E*, 2010, **82**, 041711.
17 B. Senyuk, Y.-K. Kim, L. Tortora, S.-T. Shin, S. V. Shiyanovskii and O. D. Lavrentovich, *Mol. Cryst. Liq. Cryst.*, 2011, **540**, 20–41.
18 P. Kumar, Y. G. Marinov, H. P. Hinov, U. S. Hiremath, C. V. Yelamaggad, K. S. Krishnamurthy and A. G. Petrov, *J. Phys. Chem. B*, 2009, **113**, 9168–9174.
19 E. Dorjgotov, K. Fodor-Csorba, J. T. Gleeson, S. Sprunt and A. Jákli, *Liq. Cryst.*, 2008, **35**, 149–155.
20 P. Sathyanarayana, S. Radhika, B. K. Sadashiva and S. Dhara, *Soft Matter*, 2012, **8**, 2322–2327.
21 P. Sathyanarayana, V. S. R. Jampani, M. Škarabot, I. Muševič, K. V. Le, H. Takezoe and S. Dhara, *Phys. Rev. E*, 2012, **85**, 011702.
22 G. Shanker, M. Nagaraj, A. Kocot, J. K. Vij, M. Prehm and C. Tschierske, *Adv. Funct. Mater.*, 2012, **22**, 1671–1683.
23 D. Shen, S. Diele, I. Wirt and C. Tschierske, *Chem. Commun.*, 1998, **23**, 2573–2574.
24 D. Shen, A. Pegenau, S. Diele, I. Wirth and C. Tschierske, *J. Am. Chem. Soc.*, 2000, **122**, 1593–1601.
25 R. A. Reddy, G. Dantlgraber, U. Baumeister and C. Tschierske, *Angew. Chem., Int. Ed.*, 2006, **45**, 1928–1933.
26 M. Hird, J. W. Goodby, N. Gough and K. J. Toyne, *J. Mater. Chem.*, 2001, **11**, 2732–2742.
27 K. M. Fergusson and M. Hird, *J. Mater. Chem.*, 2010, **20**, 3069–3078.
28 S. Kang, Y. Saito, N. Watanabe, M. Tokita, Y. Takanishi, H. Takezoe and J. Watanabe, *J. Phys. Chem. B*, 2006, **110**, 5205–5214.
29 W. Weissflog, U. Dunemann, S. Findeisen-Tandel, M. G. Tamba, H. Kresse, G. Pelzl, S. Diele, U. Baumeister, A. Eremin, S. Stern and R. Stannarius, *Soft Matter*, 2009, **5**, 1840–1847.
30 R. Deb, R. K. Nath, M. K. Paul, N. V. S. Rao, F. Tuluri, Y. Shen, R. Shao, D. Chen, C. Zhu, I. I. Smalyukh and N. A. Clark, *J. Mater. Chem.*, 2010, **20**, 7332–7336.
31 D. K. Yoon, R. Deb, D. Chen, E. Koerblova, R. Shao, K. Ishikawa, N. V. S. Rao, D. M. Walba, I. I. Smalyukh and N. A. Clark, *Proc. Natl. Acad. Sci. U. S. A.*, 2010, **107**, 21311–21315.
32 S.-T. Hur, M.-J. Gim, H.-J. Yoo, S.-W. Choi and H. Takezoe, *Soft Matter*, 2011, **7**, 8800–8803.
33 P. Tadapatri, U. S. Hiremath, C. V. Yelamaggad and K. S. Krishnamurthy, *J. Phys. Chem. B*, 2010, **114**, 1745–1750.
34 P. Sathyanarayana, T. A. Kumar, V. S. S. Sastry, M. Mathews, Q. Li, H. Takezoe and S. Dhara, *Appl. Phys. Express*, 2010, **3**, 091702.
35 D. D. Sarkar, R. Deb, N. Chakraborty and V. S. R. Nandiraju, *Liq. Cryst.*, 2012, **39**, 1003–1010.
36 A. Saupe, *Z. Naturforsch Pt B*, 1960, **15b**, 815.
37 H. J. Deuling, *Mol. Cryst. Liq. Cryst.*, 1972, **19**, 123–131.
38 Y. A. Nastishin, R. D. Polak, S. V. Shiyanovskii, V. H. Bodnar and O. D. Lavrentovich, *J. Appl. Phys.*, 1999, **86**, 4199–4213.
39 T. Uchida and Y. Takahashi, *Mol. Cryst. Liq. Cryst.*, 1981, **72**, 133–137.
40 W. R. Folks, Y. A. Reznikov, S. N. Yarmolenko and O. D. Lavrentovich, *Mol. Cryst. Liq. Cryst. Sci. Tech. Mol. Cryst. Liq. Cryst.*, 1997, **292**, 183–197.
41 S.-T. Wu, U. Efron and L. D. Hess, *Appl. Opt.*, 1984, **23**, 3911–3915.
42 S.-T. Wu and D.-K. Yang, *Reflective Liquid Crystal Displays*, Wiley, Chichester Eng., New York, 2001.
43 L. M. Blinov and V. G. Chigrinov, *Electrooptic Effects in Liquid Crystal Materials*, Springer-Verlag, New York, 1994.
44 J. C. Loudet, P. Hanusse and P. Poulin, *Science*, 2004, **306**, 1525.
45 H. Stark, *Phys. Rep.*, 2001, **351**, 387–474.
46 J. C. Crocker and D. G. Grier, *J. Colloid Interface Sci.*, 1996, **179**, 298–310.
47 I. I. Smalyukh, O. D. Lavrentovich, A. N. Kuzmin, A. V. Kachynski and P. N. Prasad, *Phys. Rev. Lett.*, 2005, **95**, 157801.
48 G. E. Volovik and O. D. Lavrentovich, *Zhurnal Eksperimentalnoi i Teoreticheskoi Fiziki*, 1983, **85**, 1997; *Sov. Phys. JETP*, 1983, **58**, 1159.
49 W. H. de Jeu, W. J. Goossens and P. Bordewijk, *J. Chem. Phys.*, 1974, **61**, 1985–1989.
50 W. H. de Jeu, T. W. Lathouwers and P. Bordewijk, *Phys. Rev. Lett.*, 1974, **32**, 40–43.
51 C. Zhang, M. Gao, N. Diorio, W. Weissflog, U. Baumeister, S. Sprunt, J. Gleeson and A. Jákli, *Phys. Rev. Lett.*, 2012, **109**, 107802.
52 K. Sokalski and T. W. Ruijgrok, *Physica A*, 1982, **113**, 126–132.
53 T. W. Ruijgrok and K. Sokalski, *Physica A*, 1982, **111**, 45–64.
54 H. Gruler, *Z. Naturforsch A*, 1973, **28a**, 474–483.
55 T. Warmerdam, D. Frenkel and R. J. J. Zijlstra, *J. Phys.*, 1987, **48**, 319–324.

56 P. Sathyanarayana, M. C. Varia, A. K. Prajapati, B. Kundu, V. S. S. Sastry and S. Dhara, *Phys. Rev. E*, 2010, **82**, 050701.
57 S. Kaur, J. Addis, C. Greco, A. Ferrarini, V. Görtz, J. W. Goodby and H. F. Gleeson, *Phys. Rev. E*, 2012, **86**, 041703.
58 S.-T. Wu and C.-S. Wu, *Phys. Rev.*, 1990, **42**, 2219–2227.
59 S.-T. Wu and H. T. Nguyen, *J. Appl. Phys.*, 1989, **66**, 2332–2337.
60 M. Miesowicz, *Nature*, 1946, **158**, 27.
61 M. Cui and J. R. Kelly, *Mol. Cryst. Liq. Cryst. Sci. Tech. Mol. Cryst. Liq. Cryst.*, 1999, **331**, 1909–1917.
62 D. H. McQueen and V. K. Singhal, *J. Phys. Appl. Phys.*, 1974, **7**, 1983–1987.
63 Y.-K. Kim, B. Senyuk and O. D. Lavrentovich, *Nat. Comm.*, 2012, **3**, 1133.
64 G. Toulouse, *J. Phys. Lattr.*, 1977, **38**, L67–L68.
65 M. V. Kurik and O. D. Lavrentovich, *Usp. Fiz. Nauk*, 1988, **154**, 381–431; *Sov. Phys. Usp.*, 1988, **31**, 196–224.
66 M. Kleman, *J. Phys.*, 1985, **46**, 1193–1203.